Analytic Models for Space Charge Limiting of Photoemission and Secondary Electron Emission in near-Sun Environments

M. J. Mandell, V. A. Davis, M. M. Donegan

Abstract—In geosynchronous and interplanetary environments spacecraft usually charge to positive potential due to photoelectrons emitted as a result of solar irradiation. It has long been recognized (Guernsey and Fu, 1970) that space charge barriers can form in front of the photoemitting surfaces, causing the effective photoemission to be less than what would be predicted by the spacecraft potential alone. Recently, Guillemant *et al*. (2012, 2013) and Ergun *et al*. (2010) have published PIC (particle-in-cell) calculations demonstrating that a near-Sun cylindrical spacecraft under conditions appropriate to 0.05 AU (the perihelion of Solar Probe Plus) would charge to negative potential (-16 V) due to space charge limiting of both photoelectrons and secondary electrons.

The purpose of this work is to develop an analytical treatment of photoemission and secondary electron limiting suitable for use in codes such as *Nascap-2k*, which then allows us to perform floating potential calculations for realistic spacecraft models exposed to a wide variety of near-Sun environments.

The photoemission model depends on the raw photoemission current and spectrum, the local curvature of the spacecraft surface, and the ambient environment, and is developed by fitting numeric, analytic calculations of the space charge barrier height. The model was used to calculate floating potentials of conducting spheres exposed to the Fast and Slow solar wind, as a function of distance from the sun. The spheres exhibit a fairly sharp transition from a high potential state in which effective photoemission is determined by surface potential alone, to a lower potential state due to suppressed effective photoemission by a space charge barrier. The solar distance of the transition increases with sphere radius; for a 2 meter radius sphere in the Slow solar wind a small potential reduction can be seen at 1 AU.

A related model was created for space charge limiting of secondary electrons. Both models were implemented in *Nascap-2k* and applied to near-Sun potentials of Solar Probe Plus. Predictions are that negative potentials will occur in the slow solar wind within 0.25 AU, but only close to perihelion in the fast solar wind.

Keywords—spacecraft charging, photoemission, secondary electron emission

M. J. Mandell and V. A. Davis are with Leidos, Inc., San Diego, CA, USA (e-mail: myron.j.mandell@leidos.com, victoria.a.davis@leidos.com).

M. M. Donegan is with Johns Hopkins University Applied Physics Laboratory, Laurel, MD, USA (michelle.donegan@jhuapl.edu)

I. INTRODUCTION

Charging of spacecraft in tenuous plasma at distances near or beyond 1 AU from the sun has been studied extensively for decades. It is commonly understood that electron photo-emission due to solar ultraviolet radiation dominates the current due to electrons incident from the ambient environment. This causes spacecraft to charge to positive floating potential in order to reattract the emitted photoelectrons, thus achieving current balance.

In high energy plasma (electron temperature ~ 10 keV) negative charging in sunlight can result from the negative differential charging of shaded insulators, creating negative electrostatic potential barriers in front of sunlit surfaces. However, the potential due to the photoelectron space charge itself is not, near 1 AU, strong enough to have more than a very minor effect on spacecraft potential.

Closer to the sun, however, the photoelectron density becomes high enough to form a significant barrier and cause the net photoemission current to saturate. As a spacecraft further approaches the sun, the net photoemission increases only slowly, while the incident electron current continues to increase as the inverse square with solar distance, eventually resulting in net negative current and negative spacecraft floating potential. Similar saturation of secondary electron emission current reinforces the effect.

Space charge limiting of photoemission was discussed by Guernsey and Fu [1], but only assumed importance in the context of the near-Sun mission of Solar Probe Plus. Ergun *et al*.[2] published particle simulations that showed the effect, subsequently confirmed in more extensive studies by Guillemant *et al*. [3], [4]. The objective of the current study is to develop an analytic model of space charge limiting for photoelectrons and secondary electrons suitable for use in spacecraft charging codes such as *Nascap-2k*, so that studies of charging of complex spacecraft can be performed without the need for particle tracking methods.

Section II describes the elements need for an analytic space charge barrier treatment. Section III details the treatment used for photoelectrons. Section IV describes the application of this implementation to floating potential of conducting spheres, illustrating the dependence on radius of curvature, solar wind condition, and distance from the Sun, as well as the implementation in *Nascap-2k*. Section V describes the implementation used for secondary electrons, which better accounts for lowering of the barrier by negative surface potential. *Nascap-2k* results for a cylinder and Solar Probe Plus

accounting for space charge limiting of both photoelectrons and secondary electrons with realistic geometry and material are presented in Section VI, and the results are summarized in Section VII.

II. ELEMENTS OF A TREATMENT

A barrier to low energy emitted electrons appears notionally as shown in Fig. 1. A barrier is a potential minimum that may form in front of either positive or negative surfaces. The barrier height, B, is the difference between the surface potential and the minimum potential. The negative space charge of the emitted electrons strongly dominates the positive ambient space charge from the emitting surface to a point well beyond the barrier. Beyond the barrier, the space charge density of the emitted electrons decreases sharply due to both acceleration and divergence. The two space charge densities are equal at the point where the second derivative of the potential curve changes from positive to negative. We use the nomenclature shown in Table I.
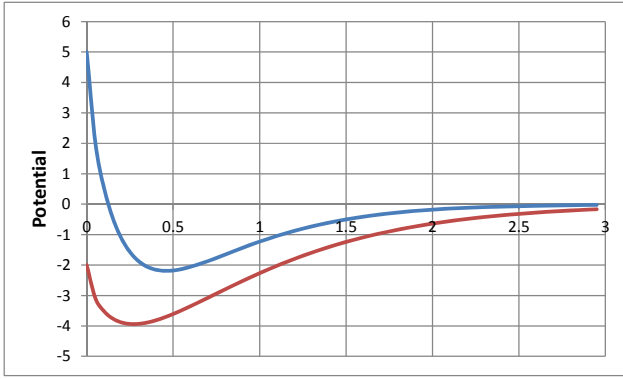

Fig. 1. Notional potential profiles for space charge barriers in front of an emitting surface.

TABLE I. NOMENCLATURE

ITEM	DEFINITION
N_A	Ambient number density (m^{-3})
T_e	Ambient electron temperature (eV)
J_{th}	Electron thermal current (Am^{-2})
V	Solar wind speed (m/s)
V_s	Surface Potential (V)
B	Barrier height (V), such that the barrier occurs at a potential V_s-B
R	Distance from the sun (AU)
R_c	Local radius of curvature of the surface (m)
φ	Local potential (v)
r_c	Radius of barrier (m)
J_0	Raw current density (Am^{-2})
$J(E)$	Current emitted with energy greater than E (Am^{-2})
$J_p(E)$	Photoemission current emitted with energy greater than E at 1 AU (Am^{-2})
T_s	Secondary electron temperature (eV), taken as 2 eV
ρ_s	Space charge at barrier due to secondary electrons
d_0	Monoenergetic limiting distance (m)
d	Approximate distance of barrier from surface (m)
θ	Incident angle of the sunlight

Since the emitted electron space charge is dominant within the barrier, we can take the barrier potential to be zero and the surface potential, V_s, to be B. The space charge density within the barrier is given as a function of potential and radial position, r, by

$$\rho(\varphi, r) = \left(\frac{R_c}{r}\right)^2 \sqrt{\frac{m}{2e}} \int_{B-\phi}^{\infty} \frac{dJ}{dE} \frac{1 + H(B-E)}{\sqrt{E - (B-\varphi)}} dE \qquad (1)$$

where the Heaviside function, $H(x)$, accounts for the return of electrons with insufficient energy to surmount the barrier. Using (1), Poisson's equation may be integrated inward from the barrier radial position to the surface to obtain the surface potential and iterated to satisfy the self-consistency condition $V_s = B$.

Using (1) alone, the barrier height increases with the barrier distance without limit. Thus, a barrier treatment requires either setting a maximum barrier radius, or establishing a relationship between the barrier and the ambient density. A sensible condition for the latter is that when the potential reaches near zero, the ambient ions are neutralized half by the incoming ambient electrons and half by the outgoing low energy electrons (since the outgoing ambient electrons are blocked by the object). This gives the following condition

$$\int_{B}^{\infty} \frac{dJ}{dE} \frac{dE}{\sqrt{\frac{2e}{m}(E-V_s)}} = 0.5 N_A e \qquad (2)$$

III. IMPLEMENTATION FOR PHOTOEMISSION

For photoemission, (2) reduces to

$$\int_{B}^{\infty} \frac{1}{J_0} \frac{dJ}{dE} \frac{dE}{\sqrt{(E-V_s)}} = \sqrt{\frac{2e}{m}} \frac{0.5 n_i e}{J_0 \cos\theta} . \qquad (3)$$

with photoemission assumed proportional to $\cos\theta$. Note that both sides of (2) are independent of distance from the Sun, assuming N_A and J_0 both have inverse square dependence. We also need to make an assumption about the spectrum of the emitted photocurrent. While recognizing that a simple Maxwellian may be adequate and would simplify the treatment, we use spectrum for 1 AU proposed by Nakagawa et al. [5]:

$$J_p(E) = 53e^{-E/1.6} + 21e^{-E/3.0} + 4e^{-E/8.9} \qquad (4)$$

The magnitude is assumed to vary as inverse square with distance from the sun. Thus $J_0 = 78 \times 10^{-6}/R^2$. We use two conditions to calculate a barrier height, and use the minimum of the two calculated barriers to determine effective photoemission and thus spacecraft surface potential:

1. Use (1) to calculate the barrier, assuming the barrier is located at the radius $\sqrt{2}R_c$. This gives the result shown in Fig. 2, where we have set a maximum barrier height of 12 V since, as we shall see, that is the maximum value obtained from the second condition below. Note that the minimum emission current shown in Fig. 2 is about 30 times that at 1 AU. The resulting barrier height depends on the raw emission current and radius of curvature, but not on the surface potential. For simplicity of application, the barrier shown in the curves in Fig. 2 is reasonably well fit by the equation

$$B_1 = \left(24.772 + 13.755 R_c - 7.6419 R_c^2\right)\left(J_0\, cos\,\theta\right)^{0.4291 - 0.1542 R_c} \quad (5)$$

where the photoemission angular dependence is explicitly included.

2. Use (2) to calculate a barrier that depends on the ratio of ambient ion density to emission current, weakly on surface potential, and not on the radius of curvature. This treatment is appropriate when the barrier is much closer to the surface than the radius posited in above condition. Fig. 3 shows the results for nominal 1 AU conditions (78 μA m^{-2} raw photoemission and 7 cm^{-3} ion density), so that the right hand side of (3) takes the value $4.26 \times 10^{-3}/cos\theta$. As noted above, the inverse square dependence of density and photoemission has been removed. It is convenient to plot the result as a function of $cos\theta$, and then scale $cos\theta$ to account for a different ratio of density to raw photoemission. Note that there is little dependence on surface potential until the surface potential becomes quite negative, so it is convenient to use a fit to the $Vs=0$ result (shown in Fig. 4) to calculate the second barrier estimate, B_2. To account for the photoemission/density ratio being different from 1 AU conditions, the equation shown in Fig.

4 is solved using the ordinate $y = \dfrac{J_0\, cos\,\theta}{78 \times 10^{-6}} \dfrac{7 \times 10^6}{N_A}$.

If the surface potential is positive, then the barrier must be at least equal to the surface potential, so that we finally have

$$B = max\left[V_s, min\left(B_1, B_2\right)\right]. \quad (6)$$

IV.   APPLICATION: SPHERE CHARGING IN SOLAR WIND

We illustrate this formulation by calculating the charging of conducting spheres in the solar wind. The purpose of this calculation is not to predict spacecraft potentials, but rather to identify the regimes in which photoemission limiting is important, and to provide data to test the implementation of this treatment in *Nascap-2k*.

The floating potential of the sphere will depend on the sphere radius, distance from the sun, and the character of the solar wind (here characterized as "Slow," "Typical," or "Fast"). The components of current to the sphere are:

1. Ion current :

$$I_{ion} = \pi R_{sphere}^2 \times N_A e V. \quad (7)$$

2. Electron current to dark side:

$$I_{e,dark} = 2\pi R_{sphere}^2 J_{th} \begin{cases} 1 + \dfrac{\phi_{sphere}}{T_e} & for\ \phi_{sphere} > 0 \\ exp\left(\phi_{sphere}/T_e\right) & for\ \phi_{sphere} < 0 \end{cases}. \quad (8)$$

3. Photoemission current (and barrier, *B*) determined as function of angle as described in Section III and integrated over the sunlit hemisphere.
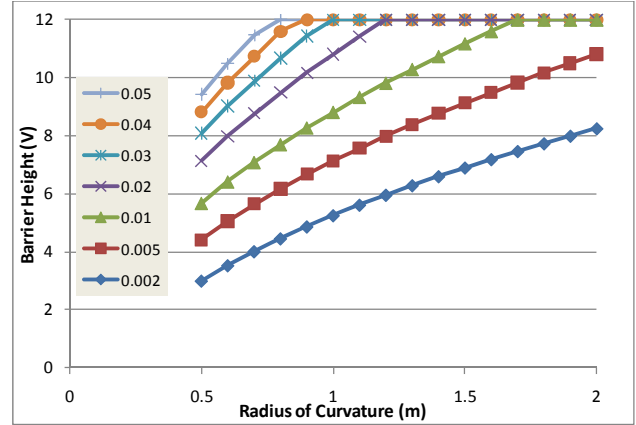

Fig. 2. Space charge barrier height calculated using condition (1) which supposes a barrier distance depending on the radius of curvature. The curves correspond to a range of raw photoemission currents (Am^{-2}) as specified in the legend.
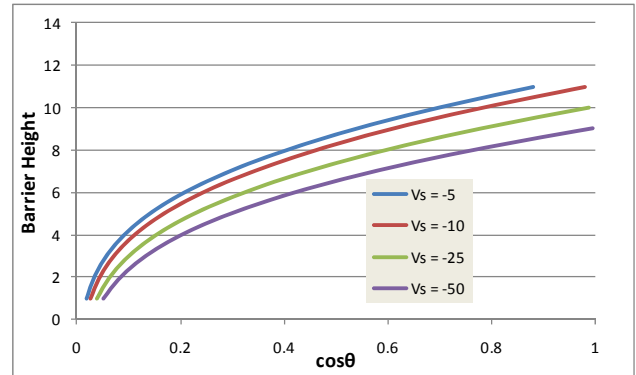

Fig. 3. Space charge barrier height calculated using condition (2) for nominal conditions at 1 AU, and for various negative surface potentials.
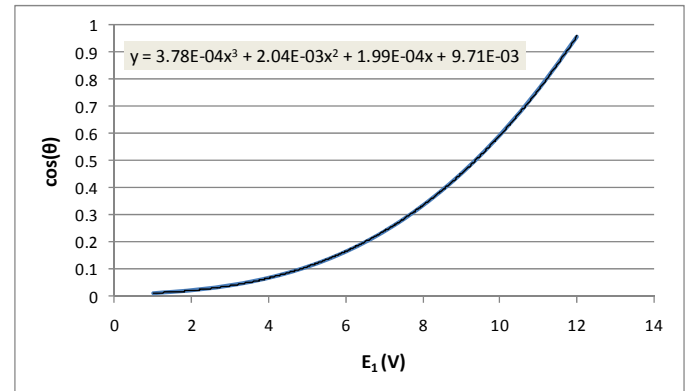

Fig. 4. Relation between barrier and angle for a zero potential photoemitting surface with nominal 1 AU conditions.

3

4. Electron current incident to sunlit side must be integrated over angle as it is a function of the barrier, B:

$$J_e = J_{th} \begin{cases} 1 + \dfrac{\phi_{sphere} - B}{T_e} & for \, \phi_{sphere} - B > 0 \\ exp\left((\phi_{sphere} - B)/T_e\right) & for \, \phi_{sphere} - B < 0 \end{cases}. \quad (9)$$

For each sphere radius, solar distance, and solar wind character the total current is calculated as a function of sphere potential and the sphere floating potential is thus determined. The parameters used in calculating the solar wind speed, density, and temperature are given in Table II.

Fig. 5, Fig. 6, and Fig. 7 give the calculated floating potentials in the Fast, Typical, and Slow solar wind respectively, ordered by increasing plasma density. In each figure there is a low potential solution close to the Sun for which photoemission is strongly space charge limited, and a high potential solution further from the Sun in which photoemission is potential limited. For each sphere radius there is a fairly sharp transition (as a function of solar distance) between the two solutions. The distance from the Sun at which the transition occurs increases with sphere radius, as the larger spheres allow barriers to form over larger distances from the surface. The low potential solution increases in prevalence with plasma density (i.e., electron thermal current) because an increasing effective photocurrent is required to balance increasing electron thermal current, and a lower barrier suffices to reduce the effective photocurrent below the required level. For the slow solar wind, the potential of a very large (2 m radius) sphere is suppressed by space charge limited photoemission even at 1 AU.

The nearly bistable structure of the potential solutions is probably unique to the spherical shape, and may not apply to realistically shaped spacecraft. Large flat areas are likely to have their photoemission reduced by space charge limiting, whereas small features or the edges of large areas will probably experience no limiting. Net photoemission is sensitive to fairly small changes in potential, so reasonable approximations should give good results for floating potential.

A. Nascap-2k Implementation

We implemented this model in *Nascap-2*k. The user can request that the model be applied. *Nascap-2k* calculates the local radius of curvature based on the laplacian potential solution.

To verify that the implementation is correct, *Nascap-2k* was used to compute the floating potentials of spheres for a few points in the above figures. The *Nascap-2k* calculations were

done with a quasispherical object. The secondary emission was suppressed by two orders of magnitude by adjusting the material properties. The backscattered electron current remained in the calculation, but was verified to have negligible effect on the result. The results, shown in Fig. 8 and Fig. 9, are consistent with those in the figures above.
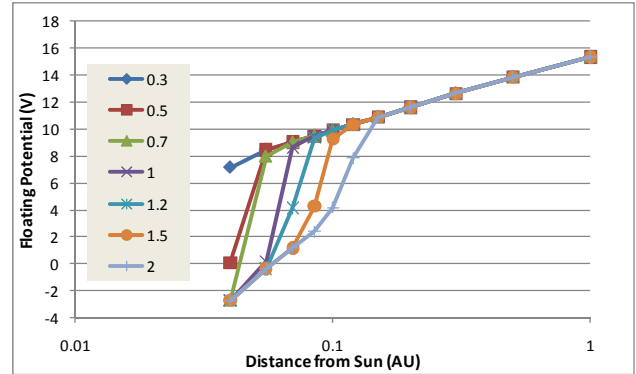

Fig. 5. Floating potential of spheres of various radii (given by legend in meters) in the Fast Solar Wind as a function of solar distance.
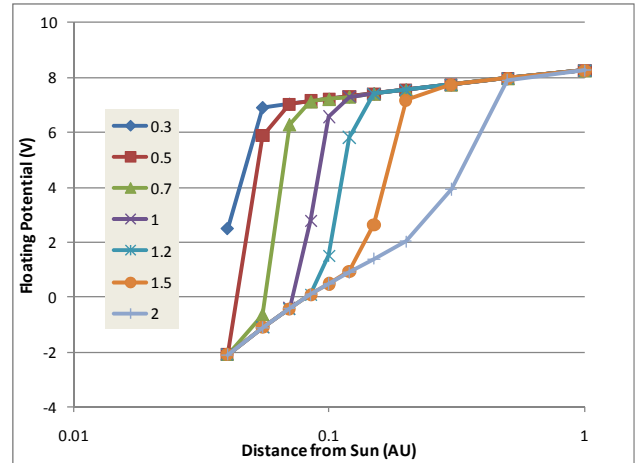

Fig. 6. Floating potential of spheres of various radii (given by legend in meters) in the Typical Solar Wind as a function of solar distance.
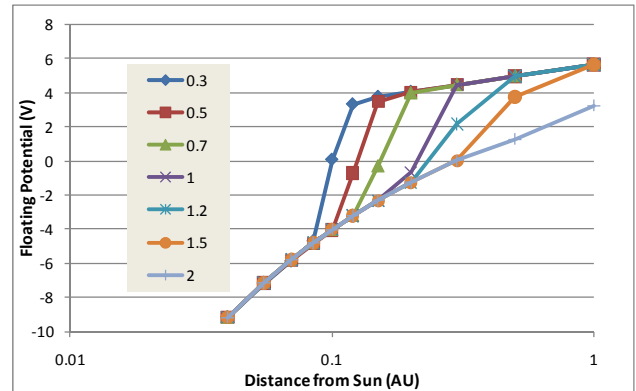

Fig. 7. Floating potential of spheres of various radii (given by legend in meters) in the Slow Solar Wind as a function of solar distance.

TABLE II. PARAMETERS USED FOR THE SLOW, TYPICAL, AND FAST SOLAR WIND. r DENOTES THE DISTANCE FROM THE SUN IN AU.

	Slow	Typical	Fast
Density (m^{-3})	$1.7\times10^7 \, r^{-2.1836}$	$7\times10^6 \, r^{-2}$	$1.75\times10^6 \, r^{-2.32}+0.0576 r^{-6.13147}$
Speed (km s^{-1})	$399 r^{-.05}$ $\times exp(-0.073 r^{-0.804})$	430	$725.6 r^{-0.01127}$
T_e (eV)	$12.5 r^{-0.456}$	$15 \, r^{-1/3}$	$9.52 r^{-0.5514}$
T_i (eV)	$4.22 r^{-0.87}$	$8 \, r^{-2/3}$	$22.7 r^{-0.56}$

4

V. IMPLEMENTATION FOR SECONDARY EMISSION

Secondary electron emission generally occurs at lower current density but higher net current (after accounting for space charge limiting and higher emission area) than photoemission. Studies by Guillemant *et al.* [3], [4] showed that the limiting of the secondary emission by the barrier played the major role in balancing incident electron current and thus determining spacecraft potential. Therefore, we elected to implement limiting of secondary electrons in a way that would emphasize the relation between barrier height and surface potential.

B. Space Charge at Barrier

We assume that at the barrier the secondary electron space charge dominates the net ambient space charge by a factor of eight. (The factor of eight is chosen to approximately fit the PIC (particle-in-cell) simulation results.) At the barrier the secondary electron current has magnitude $J_0 e^{-B/T_s}$ and has a Maxwellian distribution with temperature T_s. Its charge density is then given by $\rho_s = J_0 e^{-B/T_s} \sqrt{\dfrac{\pi m}{2eT_s}} \left(\dfrac{R_c}{R_c + d} \right)^2$, where the divergence of the electrons has been taken into account.
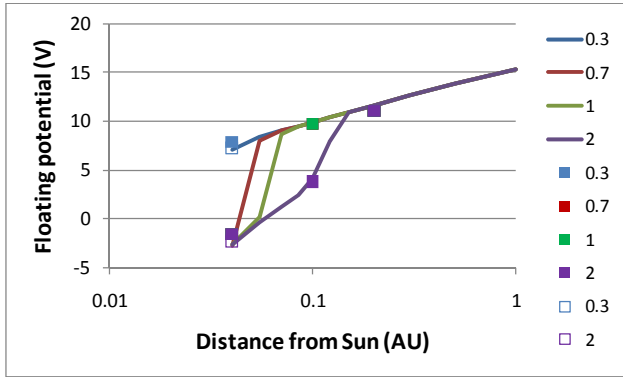

Fig. 8. Floating potential of spheres of various radii (given by legend in meters) in the Fast Solar Wind as a function of solar distance. The lines are from the Figs. 5-7 and the boxes are from the *Nascap-2k* calculations. The open boxes are for no backscattered electrons.
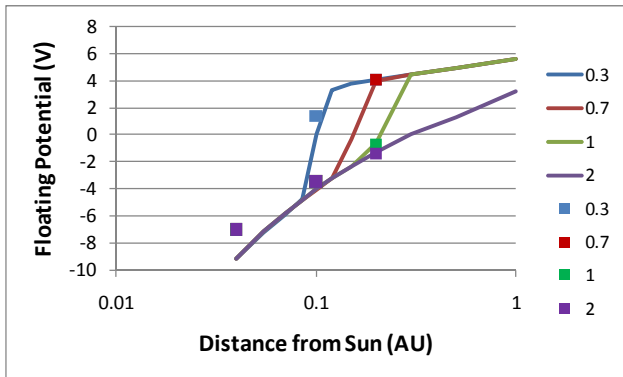

Fig. 9. Floating potential of spheres of various radii (given by legend in meters) in the Slow Solar Wind as a function of solar distance. The lines are from the Figs. 5-7 and the boxes are from the *Nascap-2k* calculations.

The ambient space charge is taken as $eN_A(1 - e^{(V_s - B)/T_e})$. Thus, the initial equation for the barrier potential becomes

$$J_0 e^{-B/T_s} \sqrt{\frac{\pi m}{2eT_s}} \left(\frac{R_c}{R_c + d} \right)^2 = 8eN_A(1 - e^{(V_s - B)/T_e}). \quad (10)$$

C. Barrier Distance

The distance of the barrier from the surface is important in order to account for divergence effects as well as the Laplace correction discussed below. For a monoenergetic emitter, the barrier distance is given by $d_0 = \sqrt{\dfrac{2.33 \times 10^{-6} T_s^{3/2}}{2J_0}}$. We can determine the barrier distance for a thermal distribution by integrating Poisson's equation inward from a barrier of assumed height. We find that the barrier distance is approximately linear with barrier height, with a distance of $3d_0$ for $V_B = T_s$. Therefore, we approximate the barrier distance as

$$d = \frac{3B}{T_s} d_0.$$

D. Laplace Correction

A charged surface has a Laplace (Coulomb) field in addition to the space charge field. For a negative surface, this Laplace field can reduce or overwhelm the calculated barrier potential.

To approximate this correction, we write the potential as a quadratic term representing the space charge plus a coulombic term representing the Laplace field:

$$\phi(r) = -B\left(1 - \left(\frac{R_c + d - r}{d} \right)^2 \right) + V_S R_c / r. \quad (11)$$

At the assumed barrier position we have

$$\phi'(R_c + d) = -V_S R_c / (R_c + d)^2$$
$$\phi''(R_c + d) = \frac{2B}{d^2} + \frac{2V_S R_c}{r^3} \quad . \quad (12)$$

If $\phi''(R_c + d)$ is negative, then the Laplace field dominates and the barrier vanishes. Otherwise, the minimum in the potential moves inward by $\Delta r = \phi'(R_c + d) / \phi''(R_c + d)$, increasing the space charge part of the field (i.e., reducing the barrier) by $B\left(\dfrac{\Delta r}{d} \right)^2$.

E. Dependence on Current, Curvature, and Plasma Density

Fig. 10, Fig. 11, and Fig. 12 illustrate the dependence of the barrier on raw secondary electron current density, radius of curvature, and ambient plasma density respectively. In each figure's legend the curves are denoted by ambient density (1×10^8 m^{-3} to 7×10^9 m^{-3}), raw secondary electron current density (1×10^{-4} Am^{-2} to 5×10^{-3} Am^{-2}), and radius of curvature

5

(0.1 m to 2 m). In all cases the secondary electron emission temperature, T_s, is 2 eV and the ambient electron temperature, T_e, is 80 eV.

Fig. 10 shows that the barrier increases with increasing raw emission current, and goes to zero at negative surface potential
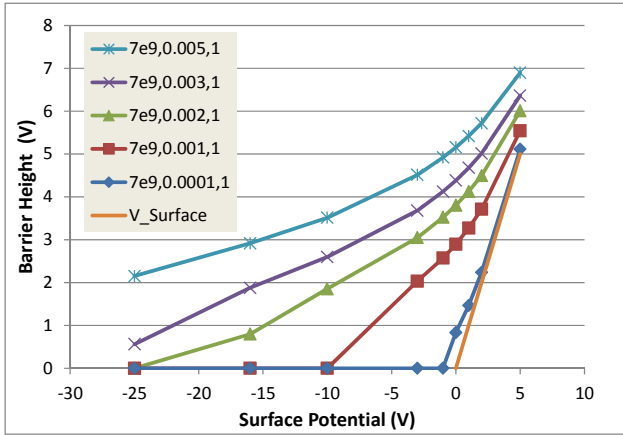

Fig. 10. Results for secondary electron barrier, illustrating the effect of raw current density. (See text).
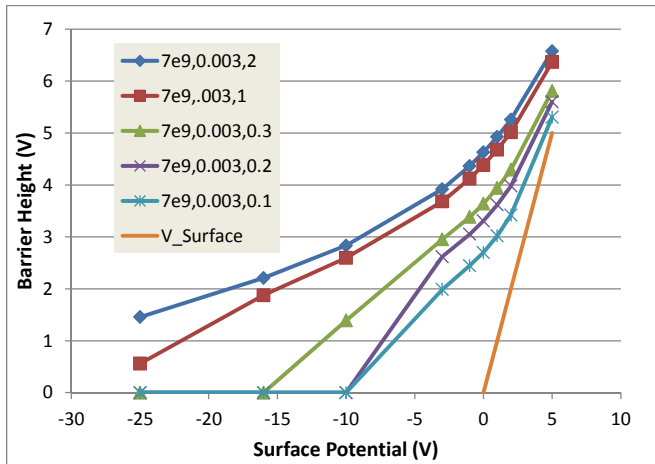

Fig. 11. Results for secondary electron barrier, illustrating the effect of local radius of curvature. (See text).
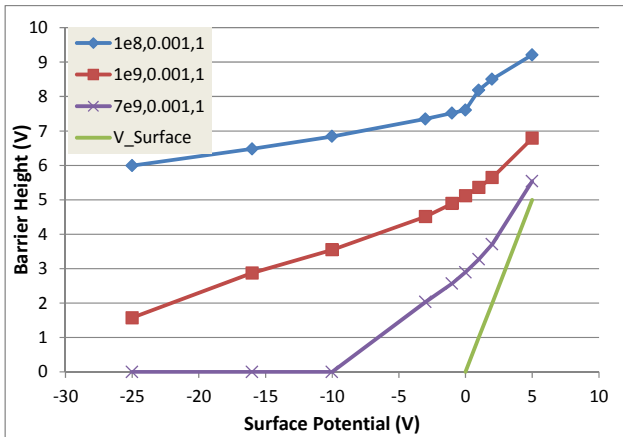

Fig. 12. Results for secondary electron barrier, illustrating the effect of ambient plasma density. (See text).

when the emission current is low. Fig. 11 shows that the barrier decreases as the surface becomes more curved due to both divergence of the emitted electrons and the Laplace correction, going to zero when the Laplace field overwhelms the space charge field. Fig. 12 illustrates the role of ambient plasma in neutralizing the space charge fields to reduce the barrier.

VI. NASCAP-2K SIMULATIONS

The above treatments have been implemented in the spacecraft charging code *Nascap-2k*, allowing charging simulations to be performed that account for both photoelectron and secondary electron space charge barriers, as well as potential barriers due to the negative potentials in the spacecraft wake.

The initial test was simulation of a conductive cylinder with conditions matching that of Guillemant *et al*. [3]. *Nascap-2k* calculated a floating potential of -13.3 V, which compares well with the previously published result of -14.5 V. The barrier to escape of low energy electrons computed using these models is 6.8 V on the Sun-facing end, between 5 and 10 V on the wake end, and between 2.4 and 3.5 V on the sides. The contributions of the spacecharge from photoemitted electrons, secondary electrons, and the ion rich wake reduce the escape of the low energy electrons. If any of these terms is excluded from the calculation, the resulting floating potential is either positive or significantly less positive.

We also did a series of calculations for a realistic geometric and material model of Solar Probe Plus. Results for nominal conditions are shown in Fig. 13. For the denser Slow solar wind we predict negative potentials within about 0.25 AU, with potential of about -10 V near perihelion. For the more tenuous Fast solar wind potentials remain positive at 0.1 AU and beyond, but may reach a few volts negative near perihelion. (The transition between 0.25 and 0.5 AU is due to the sunshade material being conductive near the Sun and insulating when far from the Sun.) Simulations for extreme conditions predict potentials as low as -30 V near perihelion. For further details see Donegan, et al, 2014 [6].
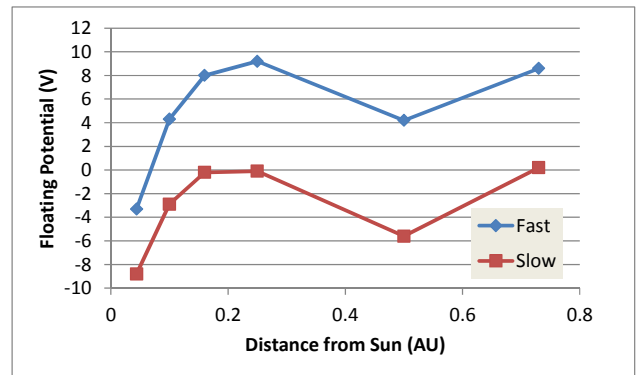

Fig. 13. *Nascap-2k* predicted floating potentials under nominal conditions in the Fast and Slow solar wind.

VII. SUMMARY

We have developed analytic models for the space charge limiting of photoelectrons and secondary electrons in the near-Sun environment. The models predict lowering of floating

6

potentials dependent spacecraft shape, emission current density, and plasma density and temperature.

The models have been implemented in *Nascap-2k*, so that sequences of calculations can be performed for realistic spacecraft models and environments. The models predict negative potentials for Solar Probe Plus within 0.25 AU in the slow solar wind, and near perihelion in the fast solar wind.

REFERENCES

[1] R. L. Guernsey and J. H. M. Fu, Potential Distribution Surrounding a Photo-Emitting Plate in a Dilute Plasma, *J. Geophys. Res., Space Physics,* 75, p. 3193, 1970.

[2] R.E. Ergun, D.M. Malaspina, S.D. Bale, J.P. McFadden, D.E Larson, F.S. Mozer, N. Meyer-Vernet, M. Maksimovie, P.J. Kellogg, J. R. Wygant, Spacecraft Charging and Ion Wake Formation in the Near-Sun Environment, *Phy. Plasma, 17*, p. 1134, 2010.

[3] S. Guillemant, V. Genot, J.C. Mateo-Velez, R. Ergun, P. Louarn, Solar wind Plasma Interaction with Solar Probe Plus Spacecraft" *Ann. Geophys. 30*, p. 1075, 2012.

[4] S. Guillemant, V. Genot, J.C. Mateo-Velez, P. Sarrailh, A. Hilgers, P. Louarn, A Simulation Study of Spacecraft Electrostatic Sheath Changes with the Heliocentric Distances from 0.044 to 1 AU , *IEEE Trans. Plasma Science,* DOI:10.1109/TPS.2013.2246193, 2013.

[5] T. Nakagawa, T. Ishii, K. Tsuruda, H. Hayakawa, T. Mukai, Net current density of photoelectrons emitted from the surface of the GEOTAIL spacecraft, *Earth Planets Space, 52*, p. 283, 2000.

[6] M.M. Donegan, V.A. Davis, M.J. Mandell, Surface Charging Predictions for Solar Probe Plus, *13th Spacecraft Charging Technology Conference*, Pasadena, CA, 23-27 June 2014.